Journal of Materials Chemistry A

ROYAL SOCIETY OF CHEMISTRY

PAPER

View Article Online
View Journal | View Issue

Cite this: J. Mater. Chem. A, 2025, 13, 36382

Impact of chitosan's degree of deacetylation, molecular weight, and crystallinity on the photoresponsive properties of azobenzene-modified films and membranes

Nils von Seggern,[a] Yannick M. Thiebes,[b] Rainer Niewa,[b] Stefan Cord-Landwehr,[c] Bruno Moerschbacher,[c] Günter E. M. Tovar[a] and Linus Stegbauer *[ad]

A profound understanding of how the degree of deacetylation (DDA), degree of polymerization (DP) and photoswitch concentration impact the photomodulation of properties of chitosan (CS)-based responsive materials can serve as a framework for future applications. Herein, we report responsive thin-films manufactured from chitosans with DDAs ranging from 70–94% and DPs ranging from 170–3380, incorporating 10–30 mol% of the light-responsive azobenzene derivative sodium-4-[(4-(2-(2-(2-methoxyethoxy)ethoxy)ethoxy)phenyl)diazenyl]-benzenesulfonate (TEGABS). During UV irradiation of the 10–30% TEGABS|CS thin-films, *e.g.* a significant increase in the indentation modulus of 10 ± 5% is observed. UV illumination leads to a decrease in water vapor permeability (WVP), which is reduced by up to 81 ± 17% compared with that of the native state. We demonstrate that TEGABS up to 10% remains as a solid-solution in CS films with differing amounts of H-aggregates depending on the DDA and DP. TEGABS at concentrations >10% in CS leads to phase separation of TEGABS crystallites with a diameter of 21 ± 8 nm. To conclude, photothermal heating by UV irradiation and the resulting water evaporation are identified as the primary driving force for the variation in mechanical properties and WVP, with photoisomerization acting as a subordinate factor. These findings provide a new pathway for the design of polysaccharide-based water vapor permeable photoresponsive membranes.

Received 30th June 2025
Accepted 12th September 2025

DOI: 10.1039/d5ta05276a

rsc.li/materials-a

[a]Institute of Interfacial Process Engineering and Plasma Technology, University of Stuttgart, Nobelstr. 12, 70569 Stuttgart, Germany. E-mail: linus.stegbauer@esm.tu-freiberg.de
[b]Institute of Inorganic Chemistry, University of Stuttgart, Pfaffenwaldring 55, 70569 Stuttgart, Germany
[c]Institute of Plant Biology and Biotechnology, University of Münster, Schlossplatz 8, 48143 Münster, Germany
[d]Biogenic Engineering Materials, TU Bergakademie Freiberg, Gustav-Zeuner-Str. 3, 09599 Freiberg, Germany

Linus Stegbauer

Prof. Dr Linus Stegbauer is a principal investigator of the Biogenic Engineering Materials group at the Institute of Nanoscale and Biobased Materials, Technical University Freiberg. Previously, he led a Liebig-funded group at the University of Stuttgart's IGVP (2019–2023) and was a DFG postdoctoral fellow at Northwestern University, USA, researching mollusk teeth biominerals. He earned his doctorate in chemistry at LMU Munich/Max Planck Institute, focusing on porous covalent organic frameworks and their environmental applications, receiving the LMU department award in 2016. He holds degrees from LMU and TU Munich, has presented at 45+ conferences, and published 20+ peer-reviewed papers.

1. Introduction

Chitosan (β-1,4-linked *N*-acetyl-D-glucosamine units (GlcNAc) and D-glucosamine units (GlcN)) has been a major focus of research, with over 110 000 publications[1] since its discovery in 1859 by C. Rouget.[2] The biopolymer chitosan, derived *via* partial deacetylation from one of the most abundant polysaccharides chitin, exhibits solubility in dilute acids with a pH below 6.5, which is achieved through protonation of the amino groups of the D-glucosamine subunit.[3] Depending on the treatment process of partial deacetylation, variations in the degree of deacetylation (DDA), molecular weight (MW) and crystallinity emerge,[4] thereby influencing the performance of the chitosan-based materials.[5]

Overall, chitosan is particularly intriguing due to its film forming ability,[6,7] biodegradability,[8] biocompatibility,[9] antimicrobial ability,[10] and mechanical properties, resembling those of common synthetic polymers.[11,12] Consequently, chitosan has been used as a membrane material in applications such as food packaging[10,13] and wound coverage.[14,15] Furthermore, chitosan has been widely utilized as an effective matrix, for instance, in the manufacturing of complex composites incorporating nanocellulose,[16,17] metal oxide nanoparticles,[18,19] or azo dyes.[20,21]

In recent years, interest in materials responsive to light as an external stimulus has increased, offering unique advantages to enhance material functionality through the implementation of a photoswitch.[22,23] Light as a trigger offers high energetic and spatiotemporal resolution, along with a non-invasive character.[24] Azobenzene and its derivatives stand out as the most prominent photoswitches, due to their efficient photochemistry, excellent reversibility, high fatigue resistance, substantial change in free volume and accessible synthesis.[25,26] Numerous studies have explored how irradiation affects the mechanical properties of smart materials, including azobenzene-containing petrobased polymers,[27–32] synthetic protein fibers,[24] liquid crystalline elastomers[33–35] and the biopolymer chitosan.[36] In addition, previous reports have indicated that the water vapor permeance can be irreversibly modified by UV irradiation.[37,38] To date, no photoresponsive biogenic membrane capable of reversibly changing water vapor permeability is known.

Currently, there is a significant gap in the utilization of polymeric matrices for light-responsive materials that meet criteria such as biocompatibility, biodegradability, and reliance on renewable resources.

Herein, we introduce a procedure for manufacturing light-responsive films containing up to 30 mol% sodium-4-[(4-(2-(2-(2-methoxyethoxy)ethoxy)ethoxy)phenyl)diazen-yl]-benzenesulfonate (TEGABS), with chitosan having a viscosity ranging from 4–460 mPa s (degree of polymerization (DP): 170 ± 24 to 3380 ± 59) and DDA varying from 70 ± 2% to 94 ± 2%. We investigate the impact of different chitosan types on the interactions between TEGABS and the polysaccharide, as well as their spectroscopic switchability, the photomodulation of the mechanical characteristics of thin films at 30% relative humidity (RH) and the application as a reversible photoresponsive membrane.

2. Results and discussion

2.1. Characterization of the chitosans involved

To refine the categorization of the TEGABS|chitosan films, size-exclusion chromatography (SEC) is applied to assess the degree of polymerization (DP) of the different kinds of chitosan, revealing a range from 172 ± 24 to 3378 ± 59 (see Fig. 1b; refer to the SI, Table S1 for details). The degree of deacetylation was taken from the datasheets provided by the manufacturer. Consequently, the following nomenclature is used for chitosans (CS) with varying DDA/DP values: 70/172 ($CS^{70/172}$), 94/226 ($CS^{94/226}$), 81/538 ($CS^{81/538}$), 86/1103 ($CS^{86/1103}$), and 84/3378 ($CS^{84/3378}$). Variations in dispersity ($Đ$) are observed among the chitosan types, ranging from 1.47 ± 0.08 for $CS^{84/3378}$ to 2.54 ± 0.20 for $CS^{81/538}$ (see SI, Table S1). By maintaining a constant DDA, the impact of the DP on the spectroscopic and mechanical properties of the $CS^{81/538}$, $CS^{86/1103}$ and $CS^{84/3378}$ films are investigated (see Fig. 1a). Simultaneously, the influence of the DDA on the sample characteristics of $CS^{94/226}$ and $CS^{70/172}$ is studied by keeping the DP steady (see Fig. 1b). The crystallinity indices (CI) of the chitosans are between 15% and 31% for all the samples except the highly crystalline $CS^{81/538}$ sample, with a value of 62% (see Fig. 1c, see SI, Fig. S1a–f). Importantly, the CIs of all our chitosan samples fall within the range reported in the literature.[39–41]

2.2. Fabrication of the TEGABS/chitosan films

TEGABS is incorporated into chitosans, ranging from 10 mol% to 30 mol% in relation to the amino functionalities of the biopolymer (see Fig. 1d).[36] A solution of TEGABS in 4 wt% aqueous acetic acid was gradually added to a chitosan (with a certain DP and DDA) solution prepared in the same solvent. After each addition step, the mixture was homogenized using a dual asymmetric centrifugal mixer (see SI, Section 1.3 for details). Aqueous acetic acid is commonly used as a solvent for chitosans due to its ability to protonate its amino groups and allow dissolution. It is important to note that as the molecular weight of the chitosan increases, the concentrations of the TEGABS and chitosan solutions are reduced. This decrease in concentration helps facilitate easier handling and prevents phase separation during mixing (see SI, Tables S2 and S3). The homogeneous solutions are casted onto etched microscope slides. The samples are first dried under a fume hood for 16 h to avoid detachment of the film before a final drying step at 35 °C for 24 h is performed. Phase separation of TEGABS in chitosan is not detected on the length scale of the microscope between cross polarizers (see SI, Fig. S2–S5, see Fig. S6 for a picture of a TEGABS crystals). Under these conditions we previously have shown that positively-charged ammonium groups of the chitosan pair with the negatively charged sulfonate groups of TEGABS.[36]

2.3. Characterization of the TEGABS/chitosan films

Nanoindentation provides insight into how the load–displacement curves are affected by the DDA, DP and TEGABS concentrations at 30% relative humidity and 20 °C (see SI, Fig. S7–S15

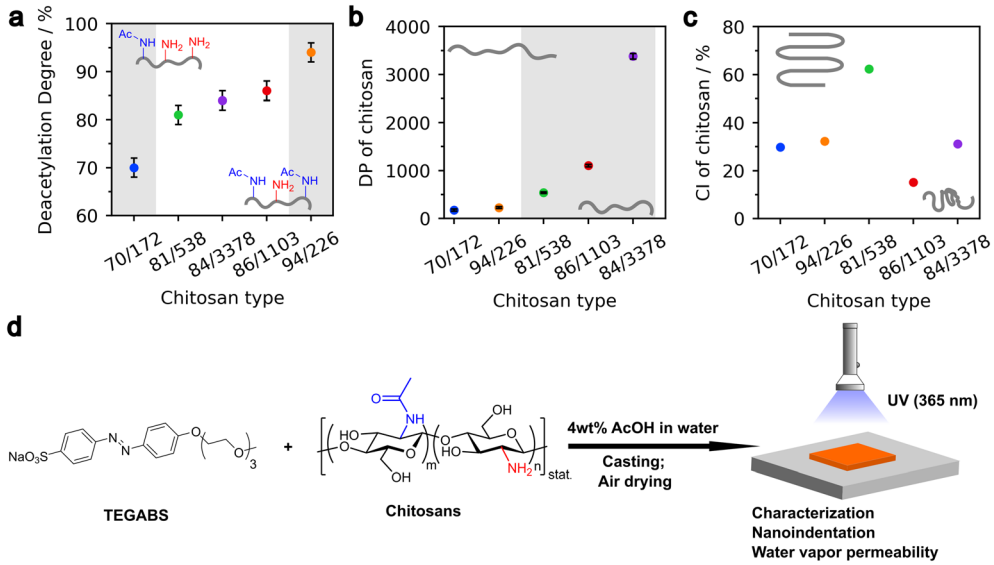

Fig. 1 Overview of the employed chitosans in this study. The degree of deacetylation (a) (given by manufacturer), the degree of polymerization (b) (determined by SEC), and the crystallinity index (c) (determined by PXRD) of employed chitosans. The gray shading indicates the classification for comparison between $CS^{70/172}$ (blue) and $CS^{94/226}$ (orange), as well as $CS^{81/538}$ (green), $CS^{86/1103}$ (red), and $CS^{84/3378}$ (violet). (d) Indicates the schematic fabrication of the material, which was established by von Seggern *et al.*[36]

and S37 for a photograph of an exemplary film). It is important to note that there is no variation in $E_{r,IT}$ or H_{IT} within replicates of the 0–30% TEGABS|CS film (see SI, Fig. S16). In the native films, the indentation modulus $E_{r,IT}$ decreases with increasing DDA at DDA < 300 by 19 ± 4% (see SI, Fig. S18), *e.g.*, *cp.* 7.0 ± 0.1 GPa in $CS^{70/172}$ *vs.* 5.6 ± 0.2 GPa in $CS^{94/226}$ (see Fig. 2a) and stays constant at DP > 500 at 5.4 ± 0.2 GPa. This finding is consistent with the findings of H. Wang *et al.*, who reported that a lower DDA leads to more chain extension, stronger intermolecular interactions and enhanced mechanical properties.[42] The stiffness of CS with a DP < 300 is due primarily to intermolecular interactions of the rod-like chains. In contrast, the stiffness of CS with a DP > 500 is derived mainly from chain entanglement.[43]

The addition of 10% TEGABS leads to a softening effect, which is strong at DP < 300 (19 ± 2% decrease in $E_{r,IT}$) and weak at DP > 500 (11 ± 2% reduction in $E_{r,IT}$). More (>10%) TEGABS lead to a linear reduction in $E_{r,IT}$ of 10 ± 3%, indicating a softening effect (see Fig. 2a and b, see SI, Fig. S18).

The rod-like arrangement of chitosan chains through intermolecular interactions, mainly contributing to the stiffness of CS with DP < 300, is disrupted by TEGABS, resulting in an increase in the free volume.[44] We hypothesize that in the low molecular weight chitosans $CS^{70/172}$ and $CS^{94/226}$, the percentage decrease in stiffness is disproportionately greater from 0% TEGABS|CS to 10% TEGABS|CS, since the mean stiffness primarily arises from intermolecular interactions of chitosan rod-like chains. In contrast, an additional contribution of chain entanglement is found in high molecular weight chitosans. In a chitosan/poly(vinyl alcohol) (PVA) blend, the robust rod-like structure of low molecular weight chitosan (M_w = 44 kDa) disappears when PVA is added due to the weakening of chitosan interactions.[45] This categorization of chitosans could be consistent with the critical entanglement molecular weights documented in the literature for synthetic polymers, such as polystyrene with 31 kDa or poly(methyl methacrylate) with 18 kDa.[46] For the polysaccharide starch, it has been established

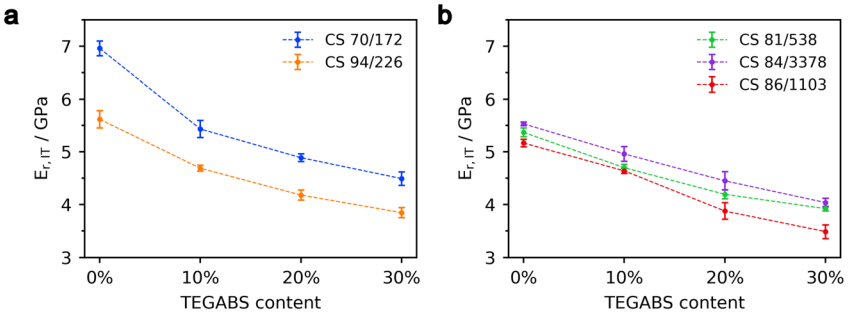

Fig. 2 Nanoindentation of native 0–30% TEGABS|CS films. Influence of different TEGABS concentrations as well as the DDA (a) and DP (b) of chitosan on $E_{r,IT}$.

that its stiffness and strength originates from a combination of chain entanglement and chain–chain interactions.[43]

Similar to $E_{r,IT}$, the indentation hardness H_{IT} of the native films at DP < 300 decreases with increasing DDA by 32 ± 3%, *e.g.*, *cp.* 236 ± 2 MPa in $CS^{70/172}$ *vs.* 160 ± 6 MPa in $CS^{94/226}$ (see SI, Fig. S17a). $CS^{84/3378}$ has the highest hardness of 196 ± 4 MPa, which is 16% greater than that of the other DP > 500 samples (see SI, Fig. S17b). We hypothesize that the low dispersity values of 1.52 ± 0.09 for $CS^{70/172}$ and 1.47 ± 0.08 for $CS^{84/3378}$ contribute to their high hardness. B. Calleja *et al.* noted that the hardness of amorphous polymers tends to diminish with increasing molecular weight and dispersity, a phenomenon attributed to an increase in free volume.[47]

The creep sensitivity reveals no distinct trends within the variations in DDA, DP, and TEGABS (see SI, Fig. S17 and S18).

2.4. Characterization of the TEGABS/chitosan films after UV irradiation

After the thin films are irradiated with UV light (365 nm, dose of 33 J cm^{-2}), nanoindentation measurements are performed. The average change after irradiation in $E_{r,IT}$ of the 10–30% TEGABS content in CS, regardless of the DDA or DP, is 10 ± 5% (see SI, Fig. S19 and 3a, b), which is consistent with previous findings of 9% for TEGABS|CS films at 30% relative humidity.[36] Other studies have indicated divergent trends in the modification of stiffness following UV irradiation of azobenzene derivative containing polymeric materials. It has been reported that the elastic modulus of a sample can be increased by 5% to 94%.[24,27,36,48,49] In reviewing the literature, a decrease in stiffness ranging from 4% to 74% was revealed, which was attributed to a light-induced reduction in the glass transition temperature.[29–31,50] The values of H_{IT} increase by 13 ± 4% for CS, regardless of DDA or DP (see SI, Fig. S20). We previously demonstrated the thermal reversibility of the mechanical properties $E_{r,IT}$ and H_{IT}.[36] The creep rate sensitivity of the DP > 500 TEGABS|CS films decreases on average by 15 ± 6% with illumination (see SI, Fig. S21). We attribute this phenomenon to the evaporation of water from the chitosan matrix. Water molecules act as plasticizers for the chitosan matrix.[36] Owing to the partial removal of water, the mobility of the entangled polymer chains of chitosan is restricted, resulting in a reduction in the creep rate sensitivity (see SI, Fig. S21).

2.5. TEGABS/chitosan water vapor membranes show reduction of transport while irradiated

We determined that upon UV irradiation, light-induced evaporation and the associated heat generation play a significant role in the behavior of the TEGABS|CS thin-films. In principle, the observed photothermal evaporation of residual moisture could influence the permeability of water vapor membranes. To investigate this possibility, we studied the water vapor permeability of CS membranes with varying DDA and DP, with and without 10% TEGABS, in the native and irradiated states (see SI for details, Fig. S22–S24). We have prepared CS thin film-membranes with a thickness of 9.9 ± 1.6 μm by casting or doctor-blading (see SI, Table S3 for thicknesses of individual membranes, Fig. S36 for a photograph of a membrane). They show a native WVP of 1.53 × 10^{-11} ± 0.17 × 10^{-11} g m^{-1} s^{-1} Pa^{-1}, with no statistically significant ($0.05 > p$) difference concerning the DDA, DP and presence of TEGABS (see Fig. 4, see SI, Fig. S25 and Table S4, for comparison with literature value, see Table S5).

Regarding the DDA and DP, the results are in agreement with the findings of Leceta *et al.* and Kim *et al.*[51,52] These results indicate that there is no significant variation in the permeability of the chitosans when the DDA is changed from 79% to 92% for membranes produced from acetic acid at a pH of 3 or when the viscosity is modified from 20–200 cP to 800–2000 cP.

Concerning the addition of TEGABS, the results are in agreement with those reported in the literature, indicating that the addition of the plasticizer glycerol to the chitosan matrix, in amounts comparable to those used in our 10% TEGABS|CS membranes, does not significantly affect the WVP.[51,53]

Upon illumination (365 nm, 55 mW cm^{-2}), when DP < 300, the 10% TEGABS|$CS^{70/172}$ and 10% TEGABS|$CS^{94/226}$ membranes show a significant decrease in WVP by 50 ± 14% regardless of the DDA, *e.g.*, from 1.39 × 10^{-11} ± 0.15 × 10^{-11} g m^{-1} s^{-1} Pa^{-1} to 0.68 × 10^{-11} ± 0.12 × 10^{-11} g m^{-1} s^{-1} Pa^{-1} and from 1.38 × 10^{-11} ± 0.17 × 10^{-11} g m^{-1} s^{-1} Pa^{-1} to 0.73 × 10^{-11} ± 0.10 × 10^{-11} g m^{-1} s^{-1} Pa^{-1}, respectively (see Fig. 4).

When the 10% TEGABS|$CS^{81/538}$ and 10% TEGABS|$CS^{86/1103}$ membranes (DP > 500) are exposed to UV-light, they show a statistically significant different decline in their WVP: 10% TEGABS|$CS^{81/538}$ declined by 81 ± 17% from 1.33 × 10^{-11} ± 0.24 × 10^{-11} g m^{-1} s^{-1} Pa^{-1} to 0.26 × 10^{-11} ± 0.18 × 10^{-11} g m^{-1} s^{-1}

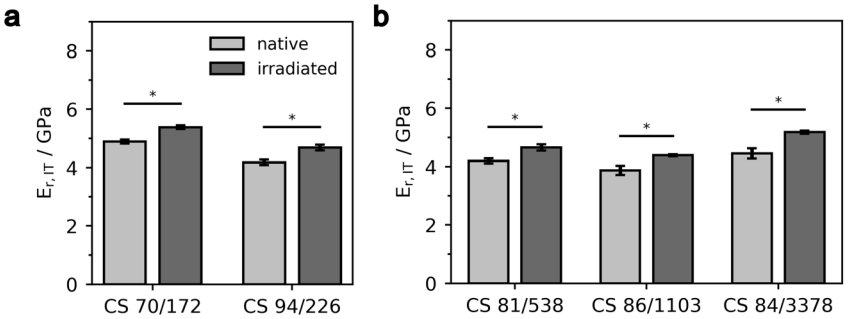

Fig. 3 Nanoindentation of 0–30% TEGABS|CS films before and after UV irradiation. Illustration of the influence of UV-light on $E_{r,IT}$ (a and b) in 20% TEGABS|CS films with varying DDA (a) and DP (b) before and after UV irradiation (λ_{exc} = 365 nm, dose of 33 J cm^{-2}). Notably, the Student's *t*-tests were conducted at a significance level of 0.01 (* = $p < 0.01$).

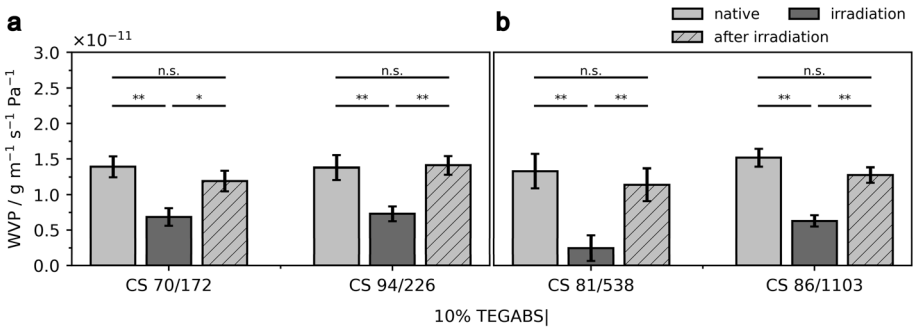

Fig. 4 Water vapor permeability measurements of 10% TEGABS|CS membranes in cup tests. Influence of UV light (365 nm, 55 mW cm^{-2}) on the WVP of DP < 300 (a) and DP > 500 (b) membranes with 10% TEGABS|CS. Notably, the Student's *t*-tests were conducted using a significance level of * = $p < 0.1$ (probability of a type-II error (β) < 0.35), ** = $p < 0.05$ and *** = $p < 0.01$.

Pa^{-1} and 10% TEGABS|$CS^{86/1103}$ declined by 58 ± 9% from 1.52 × 10^{-11} ± 0.13 × 10^{-11} g m^{-1} s^{-1} Pa^{-1} to 0.63 × 10^{-11} ± 0.12 × 10^{-11} g m^{-1} s^{-1} Pa^{-1}, respectively (see Fig. 4).

No change in WVP is observed in the pure CS films with and without UV-irradiation (see SI, Fig. S25). Upon removal of the UV irradiation, the WVP of the membranes returns to its initial value, indicating a reversible change in permeability.

The implementation of TEGABS enables the introduction of reversible modification of the WVP upon UV irradiation of the membrane. To the best of our knowledge, this is the first report of a polysaccharide-based smart membrane with reversible and temporal control over the permeability of water vapor.

We hypothesize that the photoinduced decrease in WVP can be attributed to two main mechanisms. The first process involves the photoinduced evaporation of water from the chitosan matrix,[36] leading to decreased segmental mobility due to the loss of free volume and, consequently, a lower WVP.[54,55] The second mechanism is attributed to the temperature dependence of adsorption. In general, the water vapor uptake of materials is reduced with increasing temperature,[56] *e.g.*, hydrogels[57–59] due to an increasing vapor pressure of water at higher temperatures. As a result of the selective UV absorption by TEGABS, heating occurs solely within the TEGABS|CS-membrane. As UV light penetrates and heats the entire membrane, it is assumed that water uptake is temporarily inhibited, which is expected to influence the WVP. Several reports have shown that UV light can modify barrier properties, such as the permeance of caffeine,[60] water[61] or water vapor.[37,38,62] The WVP exhibited varying trends upon irradiation in the literature. For instance, the WVP of a gelatin–chitosan-based composite film increased overall,[37] whereas that of starch–TiO_2 nanocomposites decreased.[38] However, it is important to note that the changes in permeance reported in these studies were not reversible. UV radiation induced permanent cross-linking, which lead to the observed alterations in permeance. Furthermore, the WVP was measured after illumination, unlike in this study, where it is measured during the irradiation process. Additionally, the increase in the dipole moment after *E* → *Z* isomerization of TEGABS could potentially contribute to a reduced vapor transport rate of water molecules within the film, and may thus influence both mechanical and diffusion-related properties.

Thermogravimetric analysis (TGA) indicates that upon heating (>RT), more residual water is removed in 10% TEGABS|$CS^{81/538}$ than in 10% TEGABS|$CS^{94/226}$. For example, at 55 °C, the 10% TEGABS|$CS^{81/538}$ sample loses 1% of residual water, whereas the 10% TEGABS|$CS^{94/226}$ sample loses 0.8% (see SI, Table S6 and Fig. S26). Since water acts as a plasticizer,[63] the more pronounced water removal in 10% TEGABS|$CS^{81/538}$ results in reduced chain mobility and free volume, leading to a lower WVP.

2.6. Reasoning for the photomodulated transport properties of TEGABS/chitosan films I: phase separation of TEGABS and chitosan in films

To gain a deeper understanding of the mechanism behind the photomodulation of the membrane properties, additional spectroscopic characterizations are conducted on the TEGABS|CS samples. These characterization methods include X-ray diffraction (PXRD), ultraviolet-visible spectroscopy (UV-Vis), scanning electron microscopy (SEM), and Raman spectroscopy.

PXRD is employed to examine the phase separation behavior of TEGABS in TEGABS|CS in relation to the TEGABS concentration, DDA, and DP. The deconvolution method is applied to the diffractograms to quantitatively assess phase separation (see Fig. 5a and b, see SI, Fig. S27–S29).[64] On the basis of the TEGABS content in the TEGABS|CS samples and the determined part of the crystalline TEGABS, the ratio of crystalline to solid-solution-like TEGABS in the TEGABS|CS thin films can be estimated (see SI, Section 1.11 for details).

Up to 10% TEGABS, no reflections of TEGABS are visible in TEGABS|CS. Thus, all TEGABS is present in a solid-solution-like state within the chitosan matrix, leading to the absence of TEGABS crystals in our photoresponsive membranes.

Notably, we previously reported the solid-solution-like behavior of TEGABS in the chitosan matrix.[36] Above 10% TEGABS, phase separation becomes evident in all 20% and 30% TEGABS|CS films, *e.g.*, the crystalline TEGABS content increases from 0% at 10% TEGABS|$CS^{70/172}$ to 25% at 20%

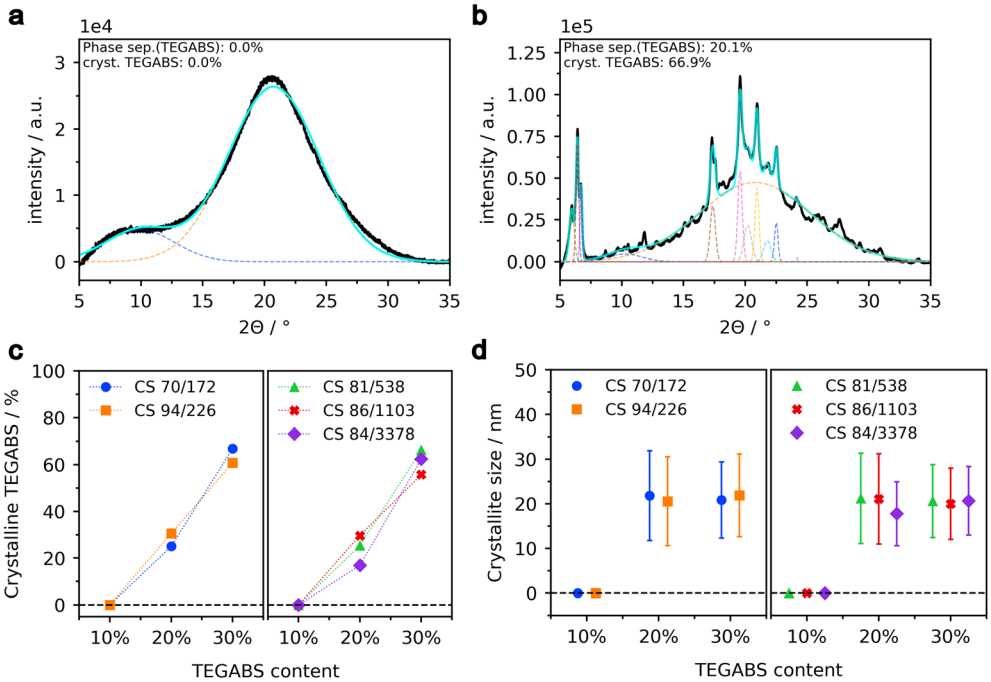

Fig. 5 Evaluation of phase separation *via* PXRD. Analysis of phase separation of crystalline TEGABS in the 10% TEGABS|CS$^{70/172}$ (a) and 30% TEGABS|CS$^{70/172}$ (b) films (see SI Section 1.11 for details, black refers to measured data, blue to fitted data with various Gaussians (other colors)). (c) Shows the fraction of phase-separated TEGABS crystals within the 10–30% TEGABS|CS matrices. (d) Illustrates the PXRD-derived crystallite size of the phase-separated TEGABS, which is calculated *via* the Scherrer equation (see SI for details).

TEGABS|CS$^{70/172}$ and further to 67% at 30% TEGABS|CS$^{70/172}$ (see Fig. 5b). No trend between the amount of crystalline TEGABS in TEGABS|CS and DP and DDA is observed (see Fig. 5c). The solubility of TEGABS in the solid-solution of TEGABS|CS is between 10% and 20% according to our data. This is consistent with the WVP results, which show no variation in permeability across any 10% TEGABS|CS thin film. The absence of TEGABS crystallinity, which would otherwise alter water vapor diffusion, accounts for this consistency.[65,66]

The average crystallite sizes of the TEGABS domains are calculated *via* the Scherrer equation. Based on sample preparation and the generally low symmetry of organic molecules,[67] it is assumed that the Scherrer equation for spherical particles also applies to our TEGABS|CS systems.

From the onset of crystalline phase separation above 10% TEGABS, the crystal size (Ø 20.6 ± 8.3 nm) remained independent of the TEGABS concentration, the DDA, and the molecular weight. Within the resolution limits of SEM, no clear morphological differences could be identified between the native and UV-irradiated states of an exemplary TEGABS/CS$^{81/538}$ film (see SI, Fig. S40).

2.7. Reasoning for the photomodulated transport properties of TEGABS/chitosan films: H-aggregation

To investigate the subtle differences between the 10% TEGABS|CS samples, we have measured 0.4–1 μm thin films (see SI, Section 1.3 for preparation, Fig. S38 for a photograph of an exemplary film) in UV-Vis spectroscopy (see SI, Fig. S30).[36] Fits by Gaussian functions (see SI, Fig. S31a) reveal that the maximum wavelength of the π–π* transition ($\lambda_{max,\pi-\pi^*}$) (see Fig. 6a and b) and the full width half maximum (FWHM) (see SI, Fig. S31b and c) are affected by the TEGABS content. For TEGABS > 10% in TEGABS|CS, we determine a hypsochromic shift and a broadening of the FWHM, *e.g.*, there is a shift from 343 nm to 332 nm and broadening from 0.74 eV to 0.91 eV as the TEGABS content increases from 10% TEGABS|CS$^{84/3378}$ to 30% TEGABS|CS$^{84/3378}$ (see SI, Table S7). The hypsochromic shift and peak broadening, observed due to the presence of both aggregated and matrix-bound dye molecules, serve as characteristic indicators of the aggregation of TEGABS molecules into H-aggregates.[68–71] Crystalline TEGABS shows a much stronger hypsochromic shift compared to TEGABS in 10% TEGABS|CS present in solid-solution. This aligns with the literature, as a pronounced hypsochromic shift from 345 nm at 10% TEGABS|CS to 329 nm at 30% TEGABS|CS was observed.[36] At 10% TEGABS, TEGABS|CS$^{81/538}$ shows the greatest bathochromic shift of 346 nm, probably indicating the lowest presence of H-aggregates.

Within the DDA category (see Fig. 6a), an increase in blue shift (*e.g.*, 343 nm for 10% TEGABS|CS$^{70/172}$ and 337 nm for 10% TEGABS|CS$^{94/226}$) and peak narrowing (*e.g.*, 0.72 eV for 10% TEGABS|CS$^{70/172}$ and 0.75 eV for 10% TEGABS|CS$^{94/226}$) indicates that a lower degree of deacetylation contributes to less TEGABS aggregation.

To conclude, UV-Vis spectroscopy qualitatively detects differing degrees of H-aggregation in solid-solution 10% TEGABS|CS thin films, which remain undetectable using PXRD (see Fig. 6c).

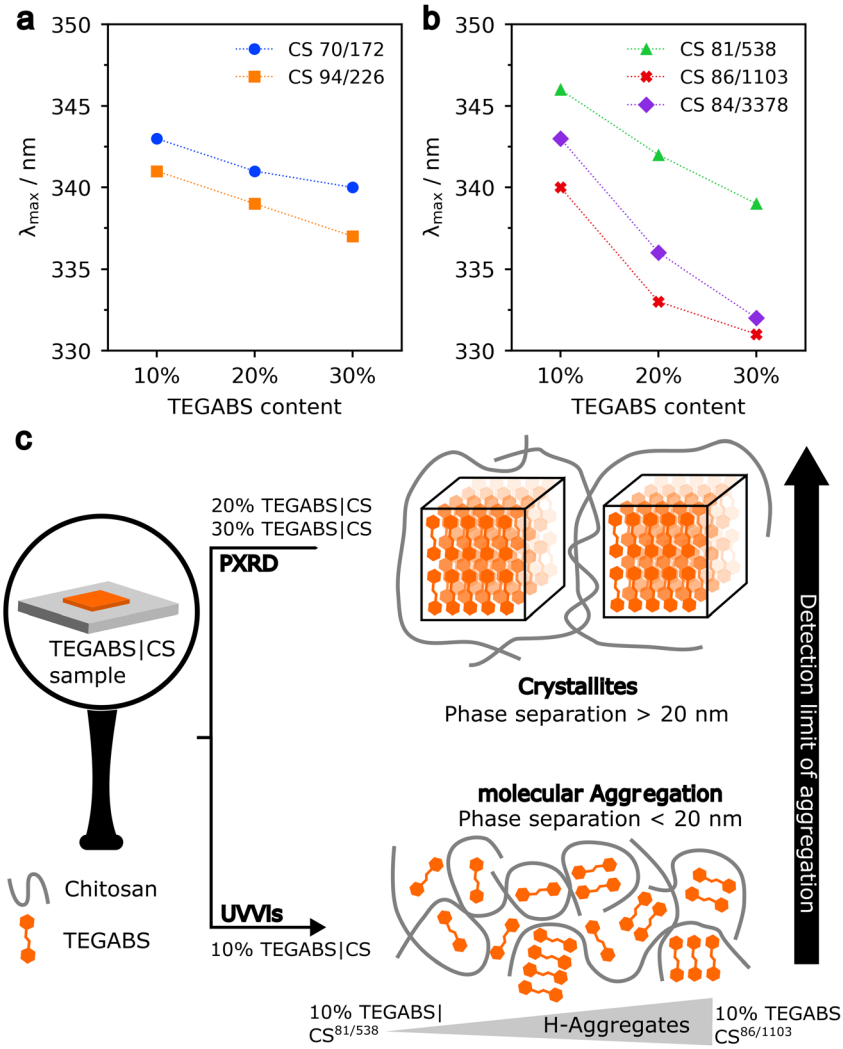

Fig. 6 UV-Vis characterization of native TEGABS|CS thin films. (a and b) UV-Vis spectra showing the wavelength λ_{max} of the π–π^* transitions of the TEGABS|CS films. (c) Indicates the two kinds of aggregates detectable *via* PXRD and UV-Vis spectroscopy. It has also been demonstrated that UV-Vis can be used to qualitatively differentiate the proportion of H-aggregates present in 10% TEGABS|CS films.

After irradiation of the films at 365 nm with a dose of 3.3 J cm^{-2} (see Fig. 7a, see SI, Fig. S39 for estimation of equilibrium dose), we observe a shift of λ_{max} of the typical π–π^* transition of the photostationary state ($PSS_{E\rightarrow Z}$), *e.g.*, for 10% TEGABS|CS$^{70/172}$ from 343 nm to 339 nm (please refer to the SI, Section 1.11 for a detailed description of the UV-Vis testing procedure for the native, irradiated, and reverted TEGABS|CS films). For TEGABS|CS$^{94/226}$, TEGABS|CS$^{81/538}$, TEGABS|CS$^{86/1103}$, and TEGABS|CS$^{84/3378}$, the decrease in intensity after irradiation changes from 47% to 35% as the TEGABS content increased from 10% TEGABS|CS to 30% TEGABS|CS (see Fig. 7b and c). This phenomenon can be explained by the increasing aggregation with a higher proportion of TEGABS, as aggregates lose the ability to undergo isomerization.[69,72] The thermal half-lives (see SI, Fig. S32 and Table S7) at 30 °C after UV irradiation are 20 h for 10% TEGABS|CS$^{94/226}$ and 29 h for 10% TEGABS|CS$^{70/172}$, indicating a faster reisomerization rate for a higher degree of deacetylation (see Fig. 7d). This can be attributed to more pronounced molecular aggregation in the 10% TEGABS|CS$^{94/226}$ film compared to the 10% TEGABS|CS$^{70/172}$ sample. The DPs do not correlate with a clear trend in the half-lives of the TEGABS|CS films (see SI, Fig. S32 and 7d).

Raman spectroscopy reveals a hypsochromic shift of the –SO_3^- stretching, independent of the chitosan type, upon increasing the TEGABS content, potentially caused by interactions *via* hydrogen bonding between the sulfonate groups of TEGABS and the ammonium groups of chitosan (see SI, Fig. S33 and S34b, c).[36] The extent of the hypsochromic shift varies within the TEGABS|CS, with a tendency to be more pronounced in higher DP TEGABS|CS, *e.g.*, from 1120 cm^{-1} for 10% TEGABS|CS$^{84/3378}$ to 1125 cm^{-1} for 30% TEGABS|CS$^{84/3378}$, compared with those with a different DDA, *e.g.*, from 1121 cm^{-1} for 10% TEGABS|CS$^{70/172}$ to 1122 cm^{-1} for 30% TEGABS|CS$^{70/172}$ (see SI, Fig. S34), which aligns with the findings of UV-Vis spectroscopy.

Given the absence of a band at 1210 cm^{-1} (gray shaded) in chitosan (see SI, Fig. S35), this region in attenuated total

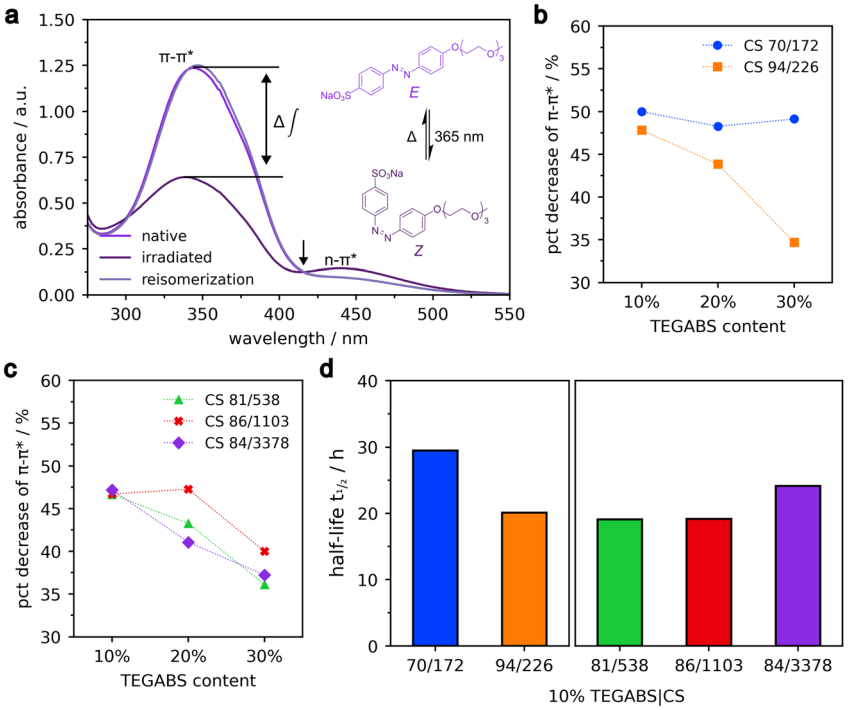

Fig. 7 UV-Vis characterization of native and irradiated TEGABS|CS thin films. In (a), the UV-Vis absorbance spectrum of the 10% TEGABS|$CS^{84/3378}$ film is depicted as native, irradiated (λ_{exc} = 365 nm, dose of 3.3 J cm^{-2}), and thermally reisomerized states. The arrow represents the isosbestic point. The percentage decrease in area for the $\pi-\pi^*$ transition from the native to isomerized state is shown for varying DDA (b) and DP (c), respectively. (d) Illustrates the influence of the DDA (left) and DP (right) on the thermal half-life of TEGABS at 30 °C.

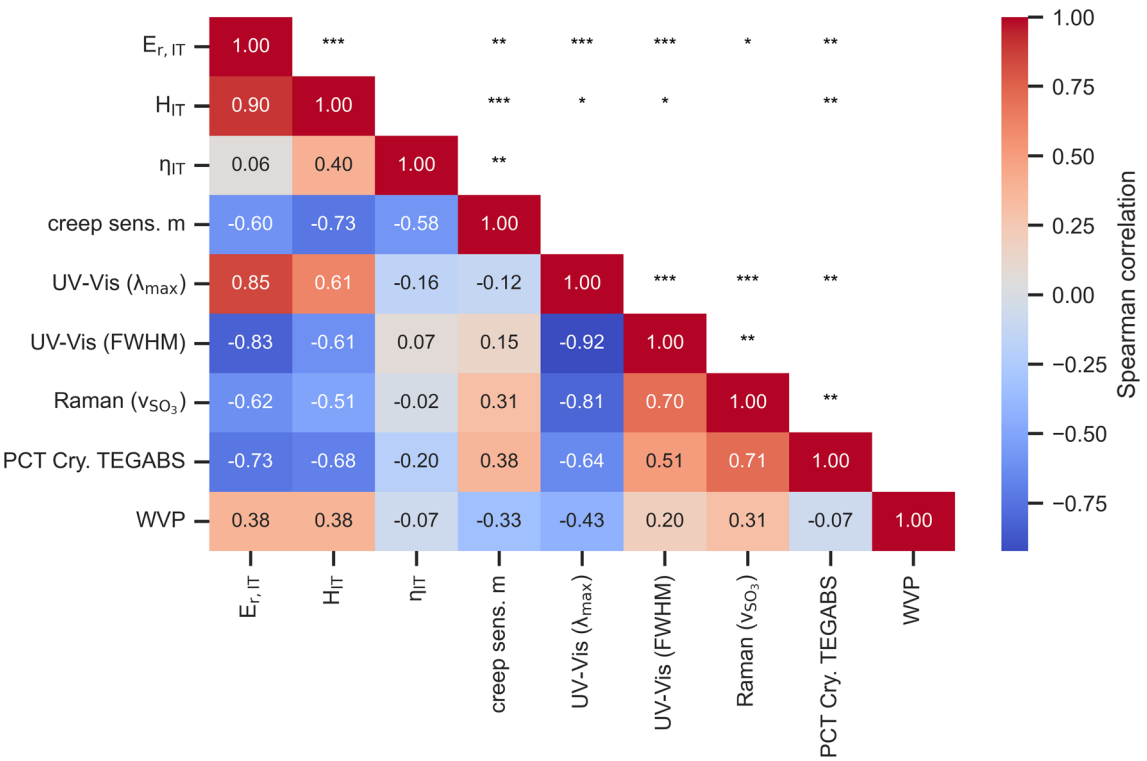

Fig. 8 Spearman correlation matrix of the (mean) values of the spectroscopic and mechanical variables measured in their native states. It should be noted that the significance levels, indicated by p-values, are shown in the upper triangle with * = $p < 0.05$, ** = $p < 0.01$ and *** = $p < 0.001$.

reflection Fourier transform infrared (ATR FT-IR) spectroscopy serves as an effective indicator for the qualitative assessment of the TEGABS content within the chitosan matrix.

To obtain the relationships between the individual measurements, a Spearman's rank correlation[73] is created. Spearman's rank correlation indicates an inverse correlation between the creep sensitivity m and both the stiffness and indentation hardness (see Fig. 8).

Moreover, alongside the correlations within the mechanical properties, the Spearman rank correlation between the spectroscopic and mechanical properties reveals that λ_{max}, $E_{r,IT}$ and H_{IT} demonstrated a strong positive correlation. A negative correlation is observed between crystalline TEGABS, FWHM (UV-Vis) and the sulfonate stretching (Raman) with stiffness, hardness and λ_{max} (see Fig. 8).

To summarize, we detected qualitatively and quantitatively two different phase separations of TEGABS in TEGABS|CS. First, in TEGABS|CS with TEGABS > 10%, the TEGABS is present as a crystalline solid independent of DDA and DP by PXRD. Second, 10% TEGABS|CS thin films show smaller hypsochromic shifts and FWHMs in the UV-Vis spectrum and presumably the lower number of H-aggregates. Among the different 10% TEGABS|CS thin films, the 10% TEGABS|$CS^{81/538}$ film has the smallest hypsochromic shift and FWHM and therefore least amounts of H-aggregates. These findings indicate that phase separation and the accompanying change in ability of TEGABS to photoisomerize do not influence the photomodulation of $E_{r,IT}$ or H_{IT}.

After two years of storage, the 10% TEGABS/$CS^{81/538}$ film exhibits a slight shift in the absorption maximum from 346 nm to 344 nm, accompanied by a ~20% increase in the full width at half maximum (FWHM) (see SI, Fig. S41). These spectral changes suggest an increase in H-type aggregation over time.

3. Conclusion

In this work, we have successfully fabricated TEGABS|CS films with 0–30% TEGABS content using five different chitosans with DDA/DP of 70/172, 94/226, 81/538, 86/1103, and 84/3378. Compared with the CSs of different DDA and DP, $CS^{70/172}$ stands out with the highest values for $E_{r,IT}$, H_{IT}, and creep rate sensitivity m. Independent of the DDA and DP, significant increases in $E_{r,IT}$ (10 ± 5%) and H_{IT} (13 ± 4%) are observed for all TEGABS-containing thin films after UV irradiation.

10% TEGABS|CS are presented for the first time as photoresponsive membranes, with the WVP decreasing in all TEGABS-containing films during UV irradiation and reversible recovery to the initial WVP within 16 h in the absence of irradiation, regardless of DP and DDA. The greatest reduction of 81 ± 17% is found for 10% TEGABS|$CS^{81/538}$. We postulate that the decrease in WVP results from the interplay between change in the dipole moment after $E \rightarrow Z$ photoisomerization, decreased water vapor adsorption caused by photothermal heating of the membrane and reduced segment mobility due to photoinduced water evaporation within the membrane.

PXRD indicates the presence of TEGABS crystallites with a diameter of 21 ± 8 nm in films containing more than 10% TEGABS. The hypsochromic shift and FWHM of the π–π* transition observed in UV-Vis reveals H-aggregates in the 10% TEGABS|CS films, with the lowest amount observed in 10% TEGABS|$CS^{81/538}$. The 10% TEGABS|$CS^{81/538}$ film also shows the highest loss of water during heating in the TGA. Altogether, we conclude that the 10% TEGABS|$CS^{81/538}$ film do show the greatest decrease in WVP because $CS^{81/538}$ seems to stabilize the solid-solution of TEGABS better, *cp.* to CS with other DDA, DP and dispersity based on H-aggregate formation observed in UV-Vis.

We have demonstrated that the photomodulation of $E_{r,IT}$, H_{IT} and the creep rate sensitivity m are not influenced by varying phase separation or photoisomerization in the 10–30% TEGABS|CS films. As a result, our conclusion is that photothermal heating by UV irradiation and the resulting water evaporation are responsible for the variation in mechanical properties, with photoisomerization acting as a subordinate factor. This study has the potential to serve as a key reference for developing smart membranes based on polysaccharides for various applications, such as responsive humidifying membranes. Moreover, the ability to reversibly modulate water vapor permeability through light irradiation introduces a dynamic and tunable functionality to thin film materials. This photodriven control could enable advanced applications in smart packaging for moisture-sensitive goods, breathable textiles that adapt to sunlight exposure, and humidity-regulating coatings for building materials or biomedical environments (*e.g.*, wounds).

Conflicts of interest

There are no conflicts to declare.

Data availability

Raw data for this article, including Origin files, python scripts are available at Open Access Repository and Archive for Research Data of Saxon Universities (Opara) at **https://doi.org/10.25532/OPARA-667**.

The data supporting this article have been included as part of the SI such as spectroscopic and mechanical data and synthesis procedures. See DOI: **https://doi.org/10.1039/d5ta05276a**.

Acknowledgements

The authors gratefully acknowledge the Carl Zeiss Stiftung (Perspective's project ChitinFluid, project P2019-02-004) and Fonds der Chemischen Industrie (Fellowship to L. S.) for their generous financial support and Shih-Yu Tseng, Samantha Wachter and Tanja Dengler for their support in conducting the experiments and sample preparation. Open access funding enabled and organized by Projekt DEAL.

References

1 *Analyze Results: Chitosan*, **https://www.webofscience.com/wos/woscc/analyze-results/583b89cd-7196-4b87-894e-5995b265867a-d870a65c**, accessed 25 March 2025.
2 C. J. C. R. Rouget, Des substances amylacées dans les tissus des animaux, spécialement des Articulés (chitine), *Comp. Rend.*, 1859, **48**, 792–795.
3 T. Hahn, E. Tafi, N. von Seggern, P. Falabella, R. Salvia, J. Thomä, E. Febel, M. Fijalkowska, E. Schmitt, L. Stegbauer and S. Zibek, Purification of Chitin from Pupal Exuviae of the Black Soldier Fly, *Waste Biomass Valorization*, 2022, **13**, 1993–2008.
4 A. Tolaimate, J. Desbrieres, M. Rhazi and A. Alagui, Contribution to the preparation of chitins and chitosans with controlled physico-chemical properties, *Polymer*, 2003, **44**, 7939–7952.
5 K. T. Hwang, S. T. Jung, G. D. Lee, M. S. Chinnan, Y. S. Park and H. J. Park, Controlling molecular weight and degree of deacetylation of chitosan by response surface methodology, *J. Agric. Food Chem.*, 2002, **50**, 1876–1882.
6 F. S. Kittur, K. R. Kumar and R. N. Tharanathan, Functional packaging properties of chitosan films, *Z. Lebensm.-Unters. -Forsch. A*, 1998, **206**, 44–47.
7 S. Gopi, S. Thomas and A. Pius, *Handbook of Chitin and Chitosan*, Elsevier, Amsterdam, 2020.
8 I. Makarios-Laham and T.-C. Lee, Biodegradability of chitin- and chitosan-containing films in soil environment, *J. Environ. Polym. Degrad.*, 1995, **3**, 31–36.
9 J. Mota, N. Yu, S. G. Caridade, G. M. Luz, M. E. Gomes, R. L. Reis, J. A. Jansen, X. F. Walboomers and J. F. Mano, Chitosan/bioactive glass nanoparticle composite membranes for periodontal regeneration, *Acta Biomater.*, 2012, **8**, 4173–4180.
10 H. Wang, J. Qian and F. Ding, Emerging Chitosan-Based Films for Food Packaging Applications, *J. Agric. Food Chem.*, 2018, **66**, 395–413.
11 B. L. Butler, P. J. Vergano, R. F. Testin, J. M. Bunn and J. L. Wiles, Mechanical and Barrier Properties of Edible Chitosan Films as affected by Composition and Storage, *J. Food Sci.*, 1996, **61**, 953–956.
12 A. Rath, B. Grisin, T. D. Pallicity, L. Glaser, J. Guhathakurta, N. Oehlsen, S. Simon, S. Carosella, P. Middendorf and L. Stegbauer, Fabrication of chitosan-flax composites with differing molecular weights and its effect on mechanical properties, *Compos. Sci. Technol.*, 2023, **235**, 109952.
13 L. Cui, S. Gao, X. Song, L. Huang, H. Dong, J. Liu, F. Chen and S. Yu, Preparation and characterization of chitosan membranes, *RSC Adv.*, 2018, **8**, 28433–28439.
14 C. Clasen, T. Wilhelms and W.-M. Kulicke, Formation and characterization of chitosan membranes, *Biomacromolecules*, 2006, **7**, 3210–3222.
15 S. Zhang, J. Li, J. Li, N. Du, D. Li, F. Li and J. Man, Application status and technical analysis of chitosan-based medical dressings: a review, *RSC Adv.*, 2020, **10**, 34308–34322.
16 H. P. S. Abdul Khalil, C. K. Saurabh, A. S. Adnan, M. R. Nurul Fazita, M. I. Syakir, Y. Davoudpour, M. Rafatullah, C. K. Abdullah, M. K. M. Haafiz and R. Dungani, A review on chitosan-cellulose blends and nanocellulose reinforced chitosan biocomposites: Properties and their applications, *Carbohydr. Polym.*, 2016, **150**, 216–226.
17 H. Celebi and A. Kurt, Effects of processing on the properties of chitosan/cellulose nanocrystal films, *Carbohydr. Polym.*, 2015, **133**, 284–293.
18 A. M. Youssef, H. Abou-Yousef, S. M. El-Sayed and S. Kamel, Mechanical and antibacterial properties of novel high performance chitosan/nanocomposite films, *Int. J. Biol. Macromol.*, 2015, **76**, 25–32.
19 X. Zhang, G. Xiao, Y. Wang, Y. Zhao, H. Su and T. Tan, Preparation of chitosan-TiO_2 composite film with efficient antimicrobial activities under visible light for food packaging applications, *Carbohydr. Polym.*, 2017, **169**, 101–107.
20 X. Cheng, Q. Zhao, D. Meng, X. Wang, J. Ma, J. Li and X. He, Chitosan/Polyvinyl Alcohol-Based Direction-Controlled Photo-Humidity Dual Responsive Membrane, *ACS Appl. Polym. Mater.*, 2022, **4**, 488–496.
21 D. S. d. Santos, A. Bassi, L. Misoguti, M. F. Ginani, O. N. de Oliveira and C. R. Mendonça, Spontaneous Birefringence in Layer-by-Layer Films of Chitosan and Azo Dye Sunset Yellow, *Macromol. Rapid Commun.*, 2002, **23**, 975–977.
22 M.-M. Russew and S. Hecht, Photoswitches: from molecules to materials, *Adv. Mater.*, 2010, **22**, 3348–3360.
23 *Analyze Results: Light-Responsive Materials*, **https://www.webofscience.com/wos/woscc/citation-report/6e173867-ba79-4e27-8303-d4dd82a2f159-877edc84**, accessed 25 March 2024.
24 J. Sun, C. Ma, S. Maity, F. Wang, Y. Zhou, G. Portale, R. Göstl, W. H. Roos, H. Zhang, K. Liu and A. Herrmann, Reversibly Photo-Modulating Mechanical Stiffness and Toughness of Bioengineered Protein Fibers, *Angew. Chem., Int. Ed.*, 2021, **60**, 3222–3228.
25 C. Dugave and L. Demange, Cis-trans isomerization of organic molecules and biomolecules: implications and applications, *Chem. Rev.*, 2003, **103**, 2475–2532.
26 J. Boelke and S. Hecht, Designing Molecular Photoswitches for Soft Materials Applications, *Adv. Opt. Mater.*, 2019, **7**, 1900404.
27 M. Moniruzzaman, P. Zioupos and G. F. Fernando, Investigation of reversible photo-mechanical properties of azobenzene-based polymer films by nanoindentation, *Scr. Mater.*, 2006, **54**, 257–261.
28 T. Srikhirin, A. Laschitsch, D. Neher and D. Johannsmann, Light-induced softening of azobenzene dye-doped polymer films probed with quartz crystal resonators, *Appl. Phys. Lett.*, 2000, **77**, 963.
29 J. M. Harrison, D. Goldbaum, T. C. Corkery, C. J. Barrett and R. R. Chromik, Nanoindentation studies to separate thermal and optical effects in photo-softening of azo polymers, *J. Mater. Chem. C*, 2015, **3**, 995–1003.
30 L. Sorelli, F. Fabbri, J. Frech-Baronet, A.-D. Vu, M. Fafard, T. Gacoin, K. Lahlil, L. Martinelli, Y. Lassailly and

J. Peretti, A closer look at the light-induced changes in the mechanical properties of azobenzene-containing polymers by statistical nanoindentation, *J. Mater. Chem. C*, 2015, **3**, 11055–11065.

31 M. Maeda, S. Nobukawa and K. Inomata, Photoinduced plasticizing effect of the addition of azobenzene on the glass transition temperature and mechanical properties of polycarbonate, *Polym. J.*, 2022, **54**, 269–279.

32 J. Vapaavuori, Z. Mahimwalla, R. R. Chromik, M. Kaivola, A. Priimagi and C. J. Barrett, Nanoindentation study of light-induced softening of supramolecular and covalently functionalized azo polymers, *J. Mater. Chem. C*, 2013, **1**, 2806.

33 M. Chen, B. Yao, M. Kappl, S. Liu, J. Yuan, R. Berger, F. Zhang, H.-J. Butt, Y. Liu and S. Wu, Entangled Azobenzene-Containing Polymers with Photoinduced Reversible Solid-to-Liquid Transitions for Healable and Reprocessable Photoactuators, *Adv. Funct. Mater.*, 2020, **30**, 1906752.

34 M. Da Pilz Cunha, E. A. J. van Thoor, M. G. Debije, D. J. Broer and A. P. H. J. Schenning, Unravelling the photothermal and photomechanical contributions to actuation of azobenzene-doped liquid crystal polymers in air and water, *J. Mater. Chem. C*, 2019, **7**, 13502–13509.

35 L. A. E. Müller, A. Demongeot, J. Vaucher, Y. Leterrier, J. Avaro, M. Liebi, A. Neels, I. Burgert, T. Zimmermann, G. Nyström and G. Siqueira, Photoresponsive Movement in 3D Printed Cellulose Nanocomposites, *ACS Appl. Mater. Interfaces*, 2022, **14**, 16703–16717.

36 N. von Seggern, N. Oehlsen, I. Moudrakovski and L. Stegbauer, Photomodulation of the Mechanical Properties and Photo-Actuation of Chitosan-Based Thin Films Modified with an Azobenzene-Derivative, *Small*, 2023, e2308939.

37 M. Rezaee, G. Askari, Z. EmamDjomeh and M. Salami, UV-irradiated gelatin-chitosan bio-based composite film, physiochemical features and release properties for packaging applications, *Int. J. Biol. Macromol.*, 2020, **147**, 990–996.

38 V. Goudarzi and I. Shahabi-Ghahfarrokhi, Photo-producible and photo-degradable starch/TiO_2 bionanocomposite as a food packaging material: Development and characterization, *Int. J. Biol. Macromol.*, 2018, **106**, 661–669.

39 E. Podgorbunskikh, T. Kuskov, D. Rychkov, O. Lomovskii and A. Bychkov, Mechanical Amorphization of Chitosan with Different Molecular Weights, *Polymers*, 2022, **14**, 4438.

40 J. Weißpflog, D. Vehlow, M. Müller, B. Kohn, U. Scheler, S. Boye and S. Schwarz, Characterization of chitosan with different degree of deacetylation and equal viscosity in dissolved and solid state – Insights by various complimentary methods, *Int. J. Biol. Macromol.*, 2021, **171**, 242–261.

41 A. Osorio-Madrazo, L. David, S. Trombotto, J.-M. Lucas, C. Peniche-Covas and A. Domard, Kinetics study of the solid-state acid hydrolysis of chitosan: evolution of the crystallinity and macromolecular structure, *Biomacromolecules*, 2010, **11**, 1376–1386.

42 H. Wang, F. Ding, L. Ma and Y. Zhang, Recent advances in gelatine and chitosan complex material for practical food preservation application, *Int. J. Food Sci. Technol.*, 2021, **56**, 6279–6300.

43 J. J. G. van Soest and N. Knooren, Influence of glycerol and water content on the structure and properties of extruded starch plastic sheets during aging, *J. Appl. Polym. Sci.*, 1997, **64**, 1411–1422.

44 M. G. A. Vieira, M. A. Da Silva, L. O. dos Santos and M. M. Beppu, Natural-based plasticizers and biopolymer films: A review, *Eur. Polym. J.*, 2011, **47**, 254–263.

45 S. Liang, Q. Huang, L. Liu and K. L. Yam, Microstructure and Molecular Interaction in Glycerol Plasticized Chitosan/Poly(vinyl alcohol) Blending Films, *Macromol. Chem. Phys.*, 2009, **210**, 832–839.

46 R. P. Wool, Polymer entanglements, *Macromolecules*, 1993, **26**, 1564–1569.

47 F. J. Baltá Calleja, A. Flores and G. H. Michler, Microindentation studies at the near surface of glassy polymers: Influence of molecular weight, *J. Appl. Polym. Sci.*, 2004, **93**, 1951–1956.

48 P. Christogianni, M. Moniruzzaman and G. Kister, Light-triggered enhancement of mechanical properties and healing effect in azobenzene-based polymer films, *Polymer*, 2015, **77**, 272–277.

49 A. Richter, M. Nowicki and B. Wolf, A Nanoindentation Study of Photo-Induced Changes in Polymers Containing Azobenzene, *Mol. Cryst. Liq. Cryst.*, 2008, **483**, 49–61.

50 B. Yang, F. Cai, S. Huang and H. Yu, Athermal and Soft Multi-Nanopatterning of Azopolymers: Phototunable Mechanical Properties, *Angew. Chem.*, 2020, **132**, 4064–4071.

51 I. Leceta, P. Guerrero and K. de La Caba, Functional properties of chitosan-based films, *Carbohydr. Polym.*, 2013, **93**, 339–346.

52 K. M. Kim, J. H. Son, S.-K. Kim, C. L. Weller and M. A. Hanna, Properties of Chitosan Films as a Function of pH and Solvent Type, *J. Food Sci.*, 2006, **71**, E119–E124.

53 S. Rivero, L. Damonte, M. A. García and A. Pinotti, An Insight into the Role of Glycerol in Chitosan Films, *Food Biophys.*, 2016, **11**, 117–127.

54 J.-F. Su, Z. Huang, Y.-H. Zhao, X.-Y. Yuan, X.-Y. Wang and M. Li, Moisture sorption and water vapor permeability of soy protein isolate/poly(vinyl alcohol)/glycerol blend films, *Ind. Crops Prod.*, 2010, **31**, 266–276.

55 A. J. Svagan, A. Åkesson, M. Cárdenas, S. Bulut, J. C. Knudsen, J. Risbo and D. Plackett, Transparent films based on PLA and montmorillonite with tunable oxygen barrier properties, *Biomacromolecules*, 2012, **13**, 397–405.

56 X. Liu, L. Zhang, B. El Fil, C. D. Díaz-Marín, Y. Zhong, X. Li, S. Lin and E. N. Wang, Unusual Temperature Dependence of Water Sorption in Semicrystalline Hydrogels, *Adv. Mater.*, 2023, **35**, e2211763.

57 H. Lu, W. Shi, J. H. Zhang, A. C. Chen, W. Guan, C. Lei, J. R. Greer, S. V. Boriskina and G. Yu, Tailoring the Desorption Behavior of Hygroscopic Gels for Atmospheric Water Harvesting in Arid Climates, *Adv. Mater.*, 2022, **34**, e2205344.

58 H. Lu, W. Shi, Y. Guo, W. Guan, C. Lei and G. Yu, Materials Engineering for Atmospheric Water Harvesting: Progress and Perspectives, *Adv. Mater.*, 2022, **34**, e2110079.
59 W. Shi, W. Guan, C. Lei and G. Yu, Sorbents for Atmospheric Water Harvesting: From Design Principles to Applications, *Angew. Chem., Int. Ed.*, 2022, **134**, e202211267.
60 K. Schöller, S. Küpfer, L. Baumann, P. M. Hoyer, D. de Courten, R. M. Rossi, A. Vetushka, M. Wolf, N. Bruns and L. J. Scherer, From Membrane to Skin: Aqueous Permeation Control Through Light-Responsive Amphiphilic Polymer Co-Networks, *Adv. Funct. Mater.*, 2014, **24**, 5194–5201.
61 E. Pantuso, G. de Filpo and F. P. Nicoletta, Light-Responsive Polymer Membranes, *Adv. Opt. Mater.*, 2019, **7**, 1900252.
62 B. Kilic, V. Dogan, V. Kilic and L. N. Kahyaoglu, Colorimetric food spoilage monitoring with carbon dot and UV light reinforced fish gelatin films using a smartphone application, *Int. J. Biol. Macromol.*, 2022, **209**, 1562–1572.
63 L. Perrin, Q. T. Nguyen, R. Clement and J. Neel, Sorption and Diffusion of Solvent Vapours in Poly(vinylalcohol) Membranes of Different Crystallinity Degrees, *Polym. Int.*, 1996, **39**, 251–260.
64 I. C. Madsen, N. V. Y. Scarlett and A. Kern, Description and survey of methodologies for the determination of amorphous content via X-ray powder diffraction, *Z. Kristallogr.*, 2011, **226**, 944–955.
65 M. Salame and S. Steingiser, Barrier Polymers, *Polym.-Plast. Technol. Eng.*, 1977, **8**, 155–175.
66 F. M. A. Leyva-Gutierrez and T. Wang, Crystallinity and Water Vapor Permeability of *n*-Alkane, Alcohol, Aldehyde, and Fatty Acid Constituents of Natural Waxes, *Ind. Eng. Chem. Res.*, 2021, **60**, 14651–14663.
67 K. D. M. Harris and P. A. Williams, in *Advances in Organic Crystal Chemistry*, ed. R. Tamura and M. Miyata, Springer Japan, Tokyo, 2015, pp. 141–166.
68 T. Moldt, D. Brete, D. Przyrembel, S. Das, J. R. Goldman, P. K. Kundu, C. Gahl, R. Klajn and M. Weinelt, Tailoring the properties of surface-immobilized azobenzenes by monolayer dilution and surface curvature, *Langmuir*, 2015, **31**, 1048–1057.
69 L. W. Giles, C. F. J. Faul and R. F. Tabor, Azobenzene isomerization in condensed matter: lessons for the design of efficient light-responsive soft-matter systems, *Mater. Adv.*, 2021, **2**, 4152–4164.
70 F. Cuétara-Guadarrama, M. Vonlanthen, K. Sorroza-Martínez, I. González-Méndez and E. Rivera, Photoisomerizable azobenzene dyes incorporated into polymers and dendrimers. Influence of the molecular aggregation on the nonlinear optical properties, *Dyes Pigm.*, 2021, **194**, 109551.
71 G. C. Fish, J. M. Moreno-Naranjo, A. Billion, D. Kratzert, E. Hack, I. Krossing, F. Nüesch and J.-E. Moser, Critical role of H-aggregation for high-efficiency photoinduced charge generation in pristine pentamethine cyanine salts, *Phys. Chem. Chem. Phys.*, 2021, **23**, 23886–23895.
72 J. M. Kuiper and J. B. F. N. Engberts, H-aggregation of azobenzene-substituted amphiphiles in vesicular membranes, *Langmuir*, 2004, **20**, 1152–1160.
73 C. Spearman, The Proof and Measurement of Association between Two Things, *Am. J. Psychol.*, 1904, **15**(1), 72–101.